MOLECULAR IMAGING AND BIOLOGY

Mol Imaging Biol (2019) 21:473–481
DOI: 10.1007/s11307-018-1228-5

Published Online: 11 July 2018

RESEARCH ARTICLE

# SPECT/CT Imaging of *Mycobacterium tuberculosis* Infection with [$^{125}$I]anti-C3d mAb

Catherine A. Foss,[1,2] Liudmila Kulik,[3] Alvaro A. Ordonez,[2] Sanjay K. Jain,[2] V. Michael Holers,[3] Joshua M. Thurman,[3] Martin G. Pomper[1,2]

[1]*The Russell H. Morgan Department of Radiology and Radiological Science, Johns Hopkins University, 1550 Orleans St. CRB2 493, Baltimore, MD, 21228, USA*

[2]*Center for Infection and Inflammation Imaging Research, Department of Pediatrics, Johns Hopkins University, Baltimore, MD, 21228, USA*

[3]*Department of Medicine, University of Colorado Denver, Aurora, CO, USA*

## Abstract

*Purpose:* Diagnosis and therapeutic monitoring of chronic bacterial infection requires methods to detect and localize sites of infection accurately. Complement C3 activation fragments are generated and covalently bound to selective bacterial pathogens during the immune response and can serve as biomarkers of ongoing bacterial infection. We have developed several probes for detecting tissue-bound C3 deposits, including a monoclonal antibody (mAb 3d29) that recognizes the tissue-bound terminal processing fragments iC3b and C3d but does not recognize native circulating C3 or tissue-bound C3b.

*Procedures:* To determine whether mAb 3d29 could be used to detect chronic *Mycobacterium tuberculosis* infection non-invasively, aerosol-infected female C3HeB/FeJ mice were injected with [$^{125}$I]3d29 mAb and either imaged using single-photon emission computed tomography (SPECT)/X-ray computed tomography (CT) imaging at 24 and 48 h after radiotracer injection or being subjected to biodistribution analysis.

*Results:* Discrete lesions were detected by SPECT/CT imaging in the lungs and spleens of infected mice, consistent with the location of granulomas in the infected animals as detected by CT. Low-level signal was seen in the spleens of uninfected mice and no signal was seen in the lungs of healthy mice. Immunofluorescence microscopy revealed that 3d29 in the lungs of infected mice co-localized with aggregates of macrophages (detected with anti-CD68 antibodies). 3d29 was detected in the cytoplasm of macrophages, consistent with the location of internalized *M. tuberculosis*. 3d29 was also present within alveolar epithelial cells, indicating that it detected *M. tuberculosis* phagocytosed by other CD68-positive cells. Healthy controls showed very little retention of fluorescent or radiolabeled antibody across tissues. Radiolabeled 3d29 compared with radiolabeled isotype control showed a 3.5:1 ratio of increased uptake in infected lungs, indicating specific uptake by 3d29.

*Conclusion:* 3d29 can be used to detect and localize areas of infection with *M. tuberculosis* non-invasively by 24 h after radiotracer injection and with high contrast.

Electronic supplementary material The online version of this article (https://doi.org/10.1007/s11307-018-1228-5) contains supplementary material, which is available to authorized users.

*Correspondence to:* Catherine Foss; *e-mail:* cfoss1@jhmi.edu

**Key words:** TB, Complement 3d, C3d, SPECT/CT, Infection imaging, Host response

## Introduction

*Mycobacterium tuberculosis* is the causative agent of tuberculosis (TB) and is responsible for 10.4 million new cases of active TB and 1.8 million deaths in 2015 alone [1]. Active TB results in illness and potential for spread while latent TB is thought to be caused by "dormant" bacteria and is non-contagious. *M. tuberculosis* is a difficult pathogen to detect and treat in that it evades the host immune system by living within alveolar and peripheral macrophages as well as within other tissues in the body including kidney, brain, and spine [2–5]. Infection with *M. tuberculosis* can also lead to the development of fibrous granulomas in lung tissue, which isolate living bacteria from pharmacotherapies, rendering treatment protracted and detection of active disease subject to sampling error and low sensitivity. Poor compliance can lead to drug resistance and higher rates of transmission. Detection of active TB at any stage is important for correct diagnosis, delineating the extent of disease and determining when it is safe to stop treatment.

The complement cascade exhibits diverse mechanisms of activation as well as selective deposition of the resulting complement cleavage products according to the molecular environment. The alternative pathway (AP) requires no antibody-antigen complex initiation and is characterized by enzymatic cleavage pathways beginning with complement 3 (C3). While the parent C3 molecule is ubiquitous, C3d, the terminal fragment of C3 cleavage, is generated in very limited circumstances [6], including some autoimmune diseases and directly by some species of bacteria, including *M. tuberculosis*. In the case of enzymatic cleavage of C3 through the AP initiated by *M. tuberculosis*, C3d is covalently bound to the outer membrane of the mycobacterium, where it modulates B cell and follicular dendritic cell-specific activation through host complement receptor (CR2) and facilitates soft entry into host macrophages through CR3 [7]. The 3d29 mAb recognizes both penultimate iC3b and the terminal fragment, C3d, each of which is covalently bound to the mycobacterium and has been used here as a direct biomarker for mycobacterial burden [6, 7]. Other pathologic conditions that generate C3d include infection with *Staphylococcus aureus* [6, 7], certain autoimmune disorders including systemic lupus erythematous, rheumatoid arthritis, age-related macular degeneration, and C3 glomerulopathies, and certain cancers [7–13]. In non-infectious cases, C3d is generated by and bound to antigens, which then largely interact with monocytes and neutrophils, which is then presented to B cells, dendritic cells, and macrophages as mentioned above. In the current study, we employ a novel imaging probe, [$^{125}$I]3d29 mAb, to detect and localize *M. tuberculosis* infection in a rodent pulmonary model using single-photon emission computed tomography (SPECT)/X-ray computed tomography (CT) imaging.

## Methods

### *Animal Model*

All procedures were conducted using Johns Hopkins University Animal Care and Use Committee-approved protocols. Female C3HeB/FeJ mice (Jackson Labs, Bar Harbor, ME) were prepared and housed as described previously [14, 15]. Mice were aerosol-infected with frozen stocks of *M. tuberculosis* H37Rv, using the Middlebrook Inhalation Exposure System (Glas-Col). At least three mice were sacrificed 1 day after infection and at the imaging time points to determine the number of implanted bacilli in the lungs. The entire lungs were harvested from infected animals, homogenized in PBS, and plated by serial dilution onto Middlebrook 7H11 selective plates (Becton Dickinson). All plates were incubated at 37 °C for 4 weeks to determine bacterial burden. A separate group of ten animals, from the same infected cohort, were used for SPECT/CT ($n = 3$) and biodistribution studies ($n = 6$), while one mouse was infected for *ex vivo* fluorescence microscopy. Four mice were left uninfected to serve as healthy controls for SPECT/CT (n = 3) and *ex vivo* fluorescence microscopy ($n = 1$). Infected mice were used between 8 and 10 weeks post-infection. All mice were 18–20 weeks of age. Day 1 post-infection colony-forming units (CFUs) were $\log_{10}$ 1.93 ± 0.12 for all of the mice used in these experiments. At the time of imaging, the average CFU was $\log_{10}$ 7.8 ± 0.24.

### *Radiolabeled 3d29 mAb and Isotype Control*

Purified, carrier-free 3d29 [9] and isotype mAb (murine $IgG_{2a}$, ab170191, Abcam, Cambridge, MA) were labeled using the Iodogen™ method [16]. Briefly, a glass vial was freshly coated with Iodogen™ reagent (Pierce-Thermo Scientific, Waltham, MA), according to the manufacturer's instructions. A 100-µl solution of 100 µg of 3d29 or isotype in PBS was added to the source vial of carrier-free, concentrated (37 MBq/µl) [$^{125}$I]NaI (Perkin Elmer, Waltham, MA) and that solution was immediately added to the Iodogen-coated vial. The labeling reaction proceeded for 12 min at ambient temperature and was then applied to the top of a PBS-conditioned Sephadex G-25 size exclusion column (GE, Fairfield, CT). The column was conditioned and eluted per manufacturer's instructions and radiolabeled antibodies were stored on ice prior to subsequent injection. Radio thin layer chromatography (TLC) using the Gelman strips (Gelman Life Sciences, Ann Arbor, MI) developed in acetate citrate dextrose buffer (Sigma-Aldrich, St. Louis, MO) indicated radiochemical purity (≥ 92 %).

### *Fluorescent 3d29 mAb and Immunofluorescence*

One hundred micrograms of 3d29 was brought to 100 µl with PBS, pH 7.4 in a microcentrifuge tube. One microliter of a stock solution of IRDye680RD-NHS (50 mg/ml in DMSO, LI-COR Biosciences, Lincoln, NE) was then added to the antibody solution and the labeling reaction proceeded at ambient temperature for 12 min. Unincorporated dye was removed as described above using Sephadex G-25 size exclusion columns. Antibody purity was tested using the Whatman 60 Å silica TLC (Sigma-Aldrich), developed in acetonitrile with UV/vis detection (≥95 %). Lung tissues from *M. tuberculosis*-infected C3HeB/FeJ mice were harvested following systemic perfusion with PBS and subsequent isoflurane-eased euthanasia induced by cervical dislocation. The lungs were fixed for 24 h in 10 % formalin, embedded in paraffin, and sectioned to 4 µm on charged glass using a standard microtome. The slides were probed with the following primary and fluorescent secondary antibodies: 3d29-IRDye680RD (1:67), macrophage (primary: anti-CD68—Abcam ab53444, 1:40; secondary: sheep anti-rat-IgG-FITC antibody—Abcam ab6848–1, 1:250) and nuclear staining (Hoechst 33342; Fisher Scientific—1 ng/ml). The primary antibodies were probed simultaneously in 10% fetal bovine serum in PBS and viewed using a Nikon 80i upright epifluorescence microscope equipped with a Nikon DS-Qi1Mc darkfield CCD camera and excited by a Nikon Intensilight C-HGFI lamp. All images were recorded and processed using Nikon Imaging Software Elements.

### *SPECT/CT Imaging*

Mice infected with *M. tuberculosis* for 10 weeks and age-matched healthy controls were injected intraperitoneally with 85.1 ± 7.4 MBq (5.55 MBq/µg) (2.3 ± 0.2 mCi, 150 µCi/µg) of [$^{125}$I]3d29 mAb or 55.5 ± 7.4 MBq (1.37 MBq/µg) (1.5 ± 0.2 mCi, 37 µCi/µg) of [$^{125}$I]isotype antibody and scanned using a Mediso NanoSPECT/CT imager (Budapest, Hungary) 24 and 48 h after radiotracer injection. The mice were scanned within biocontainment tubes equipped to deliver 1.75 % isoflurane in oxygen flowing at 2 l/min as described previously [17]. Images were acquired over 24 projections using 75 s/projection and the data were reconstructed using the manufacturer's software. All images were viewed and displayed using AMIDE software http://amide.sourceforge.net/. Three-dimensional isocontours of lung and splenic lesions were generated in AMIDE using a threshold of 1.5 % ID/g. Visual inspection of contours revealed high fidelity of lesion inclusion for subsequent summation of SPECT data to produce lesion means, and deviations.

### *Ex Vivo Biodistribution*

Six *M. tuberculosis*-infected mice and three healthy control mice were injected intraperitoneally with either 555.0 ± 5.6 kBq (15 ± 1.5 µCi, 150 µCi/µg) of [$^{125}$I]3d29 ($n = 6$) or the same amount of radioactivity of isotype control (1.67 MBq/µg, 45 µCi/µg, $n = 3$), as indicated. The mice were sacrificed 24 h following radiotracer injection by cervical dislocation followed by rapid removal and weighing of selected tissues before placing each tissue in 10-ml Falcon tubes (Fisher Scientific, Franklin, NJ) containing formalin (Fisher Scientific). Tissues were left to disinfect for 24 h prior to counting each tube in an automated gamma counter (LKB Compugamma CS 1282, Mt. Waverly, Victoria). Tissue counts were compared to a 1:10 diluted standard and percent injected dose per gram (%ID/g) of wet tissue per body weight (standardized uptake values (SUVs)) were calculated for each tissue. Percent injected dose per organ per body weight values for two tissues were also calculated to normalize for variable edematous lung weights due to infection heterogeneity.

### *Statistics*

*P* values were calculated using Microsoft Excel using a paired, two-tailed *t* test where $P \leq 0.05$ was considered to be statistically significant.

## Results

### *SPECT/CT Imaging of Infected and Healthy Mice with [$^{125}$I]3d29 and [$^{125}$I]IgG$_{2a}$ (Isotype)*

Two healthy mice and two mice infected with *M. tuberculosis* were injected with [$^{125}$I]3d29 while another pair of healthy and infected mice were injected with [$^{125}$I]IgG$_{2a}$ isotype. The mice were imaged using SPECT/CT at 24 and 48 h post-injection. At 24 h post-injection, 3D maximum intensity projections (MIPs) of healthy mice injected with [$^{125}$I]3d29 showed a small amount of uptake in the spleen (S) as well as in the thyroid (T) due to *in vivo* dehalogenation (Fig. 1a) of the radiolabeled antibody [18–20]. Otherwise, all other healthy tissue uptake was low (1.2 % ID/g). Mice infected with *M. tuberculosis* that were injected with [$^{125}$I]3d29 showed discrete, focal uptake in the lungs (lesion range 6.9–18 % ID/g) and within hypertrophied spleen (range 3–5 % ID/g) (Fig. 1b) as well as free radioiodide in the thyroid. Superficial cervical lymph nodes are also visible. Figure 1c, e (also Suppl. Fig. 1; see electronic supplementary material: ESM) depicts SPECT/CT slices in three planes showing [$^{125}$I]3d29 overlay with CT-opaque pulmonary lesions. At 48 h post-injection (Fig. 2a), healthy mice again displayed low radiotracer uptake in the spleen (S) along with thyroid (T) uptake of radioiodide while remaining tissues were clear. Infected mice (Fig. 2b) displayed radiotracer uptake in the lungs and spleen (S) but in a less discrete pattern than at 24 h. Kidney (K) uptake was also apparent as well as radiotracer within thyroid. Figure 2c–e (also Suppl. Fig. 2, ESM) shows SPECT/CT slices in three planes demonstrating less discrete uptake of

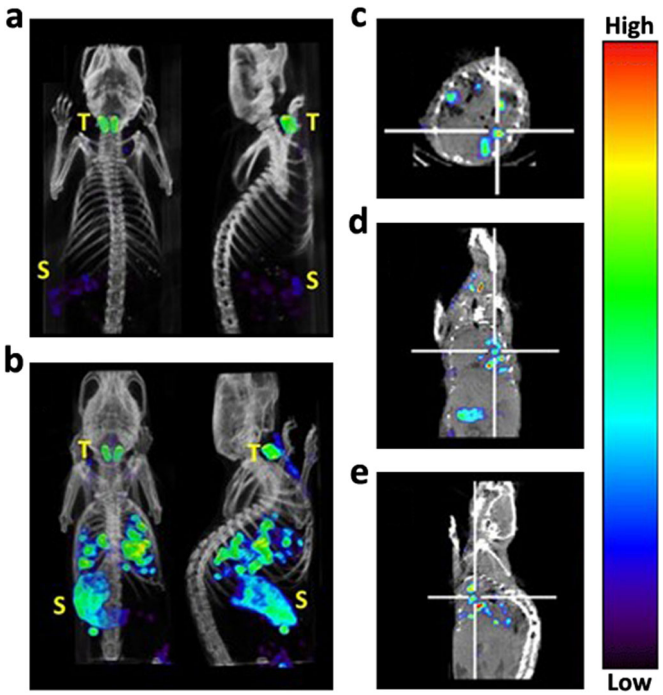


**Fig. 1.** SPECT/CT imaging of uninfected and TB-infected mice with [$^{125}$I]3d29 at 24 h post-injection. **a** Coronal and sagittal MIP images of a healthy mouse showing slight uptake at the head of the spleen (S) and metabolized radioiodine uptake in the thyroid (T). **b** Coronal and sagittal MIP images of an *M. tuberculosis*-infected mouse showing focal lung uptake along with strong uptake in inflamed spleen (S). Metabolized radioiodine uptake in the thyroid (T) is also apparent. **c** Transaxial, **d** coronal, and **e** sagittal slices, respectively, of the mouse depicted in **b** showing overlay of radiotracer signal with CT-opaque granulomas in lung. White crosshairs show a selected lesion in each slice representation.

radiotracer in infected lungs with a TB lesion identified by white crosshairs.

*M. tuberculosis* infected and healthy mice were similarly imaged using radioiodinated isotype control antibody to delineate non-specific uptake of injected murine $IgG_{2a}$ immunoglobulin. Figure 3a shows coronal and sagittal MIPs of a healthy mouse at 24 h post-injection. Stomach (St) and thyroid (T) are the only tissues showing signal and represent radioiodide [21]. Infected mice imaged at 24 h (Fig. 3b) showed thyroid, stomach, and urinary bladder. Figure 3c shows a healthy mouse imaged at 48 h demonstrating only thyroid signal. In Fig. 3d, the infected mouse at 48 h post-injection also demonstrated uptake only within thyroid.

## *Ex vivo biodistribution of [$^{125}$I]3d29 and [$^{125}$I]$IgG_{2a}$ in healthy and M. tuberculosis-infected mice*

Figure 4 shows a graph of [$^{125}$I]3d29 uptake in selected infected and healthy mouse tissues depicted as standardized uptake values (SUVs) except the one noted by an asterisk. The asterisk values are %ID per whole organ to offset the substantially increased and variable edema present in infected lungs. Across the tissues assayed, there was no statistically significant difference ($P < 0.05$) in uptake between 3d29 and isotype control antibodies in control tissues. A 3.3-fold increase in whole lung (lung*) uptake of 3d29 over isotype in TB mice as well as for 3d29 in TB over healthy mice was observed, but was not statistically significant. Additionally, a nearly 2:1 difference in 3d29:isotype uptake in kidney and muscle was observed. Healthy mice showed an increased white fat (SUV) uptake of [$^{125}$I]3d29 (3.98:1) compared with isotype and 3d29 uptake in mice infected with *M. tuberculosis*. Healthy adult C3HeB/FeJ are known for autoimmune etiologic obesity [22] while *M. tuberculosis*-infected mice have little observable body fat.

## *Immunofluorescence microscopy of M. tuberculosis-infected and non-infected mouse lung*

Sections of lungs taken from infected and healthy mice were probed with anti-CD68 antibody to delineate all phagocytic cells and fluorescently labeled 3d29 to determine the cellular distribution of C3d/iC3b in *M. tuberculosis*-infected and healthy lungs. Figure 5 shows *M. tuberculosis*-infected (Fig. 5a) and non-infected (Fig. 5b) lungs. Alveoli are evident in both panels and are ringed by green CD68+ type II pneumocytes [23], which directly harbor *M. tuberculosis*

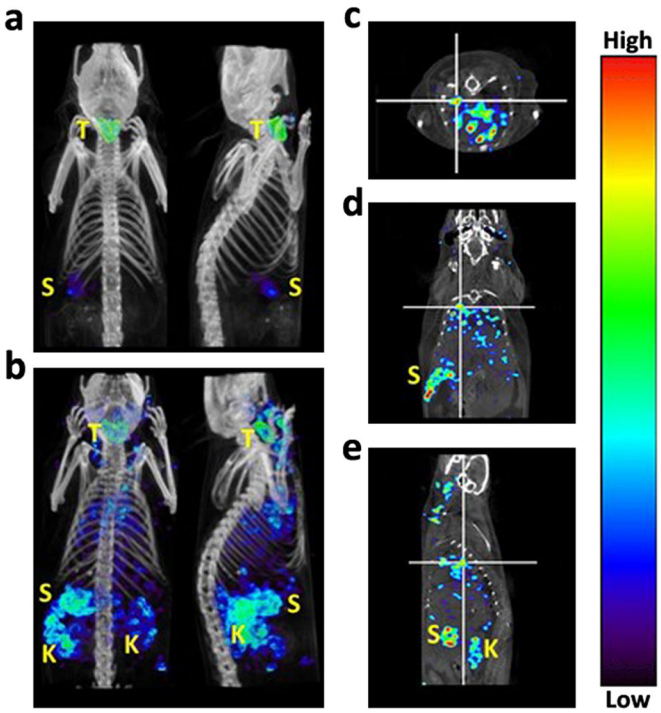


**Fig. 2.** SPECT/CT imaging of uninfected and TB-infected mice with [$^{125}$I]3d29 at 48 h post-injection. **a** Coronal and sagittal MIP images of a healthy mouse showing slight uptake at the head of the spleen (S) and metabolized radioiodine uptake in the thyroid (T). **b** Coronal and sagittal MIP images of an *M. tuberculosis*-infected mouse showing diffuse lung uptake along with strong uptake in inflamed spleen (S). Diffuse signal is now present in the kidney, reflecting metabolism of radiolabeled 3d29. Metabolized radioiodine uptake in the thyroid (T) is also apparent. **c** Transaxial, **d** coronal, and **e** sagittal slices, respectively, of the mouse depicted in (b) showing overlay of radiotracer signal with CT-opaque granulomas in lung. White crosshairs show a selected lesion in each slice representation.

infection and secrete immunomodulatory biomolecules including complement 3 [24, 25]. C3d/iC3b are stained in red by 3d29 while nuclei are represented in blue. Panel a shows intense red C3d/iC3b staining throughout the type II pneumocytes (arrows), within alveolar macrophages (arrow heads) and less intensely, within the interstitial space of the infected lung. Panel b shows a similar pattern although with markedly reduced red 3d29 staining intensity. Supplemental Figs. 3 and 4 (in ESM) show 3d29 staining in alveolar and parenchymal macrophages in interstitial lung and a higher magnification of minimal 3d29 staining of luminal type II pneumocytes, respectively.

## Discussion

Here, we have described direct imaging of complement-coated *Mycobacteria* in a mouse model of pulmonary TB. This was achieved by using a direct tyrosyl radioiodination of 3d29, a murine $IgG_{2a}$ antibody specific for C3d/iC3b fragments. *In vivo* SPECT/CT imaging in infected and healthy mice 24 h after [$^{125}$I]3d29 administration (Fig. 1) showed discrete foci of radiotracer uptake in the lungs of infected mice along with strong signal in the enlarged spleen. Both infected and uninfected mice showed thyroid uptake of metabolized radiotracer, reflecting radioiodide import and fixation [19, 20] while the uninfected mouse showed a small amount of radiotracer uptake in the spleen, a phenomenon observed previously [26]. SPECT/CT imaging at 48 h (Fig. 2) showed the same uptake pattern in healthy mice (Fig. 2a) but a much more diffuse pattern of uptake in the lungs of infected mice (Fig. 2b). Spleen uptake (S) is still apparent in the infected mice while kidney uptake (K) was also apparent. SPECT/CT images of radiolabeled isotype control in both *M. tuberculosis*-infected and healthy mice (Fig. 3) showed no lung uptake in infected or healthy mice but does show intense stomach (St) and thyroid (T) uptake of radioiodide in healthy and infected mice (Fig. 3a, b). By 48 h following [$^{125}$I]$IgG_{2a}$ administration, only thyroid uptake was visible in both mice (Fig. 3c, d), reflecting organified radioiodine. *Ex vivo* biodistribution in healthy and infected mice with either [$^{125}$I]3d29 or [$^{125}$I]$IgG_{2a}$, as indicated (Fig. 4), at 24 h post-administration revealed no significant difference in uptake between 3d29 and isotype antibodies in infected mice, likely due to $n = 3$/group small sizes and heterogeneity of disease. However, the average whole lung SUV ratio of 3d29: isotype in infected mice was 3.3:1.No other tissue comparisons among infected mice for 3d29: isotype exhibited ratios $> 2$. Discrepancies between biodistribution data and SPECT images, such as visibility of kidneys in

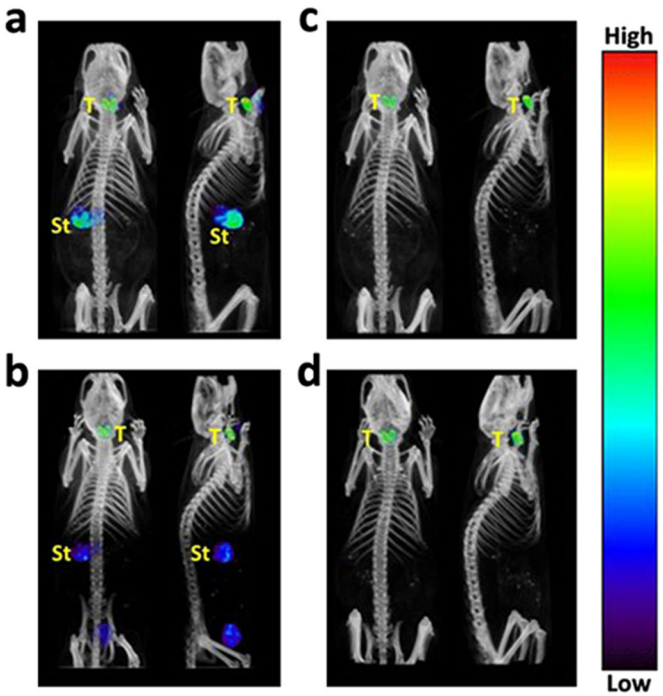


**Fig. 3.** SPECT/CT imaging of uninfected and TB-infected mice with [$^{125}$I]IgG$_{2a}$ isotype at 24 and 48 h post-injection. **a** Coronal and sagittal MIP images of a healthy mouse showing uptake of metabolized radioiodine in the stomach (St) and metabolized radioiodine uptake in the thyroid (T). **b** Coronal and sagittal MIP images of an *M. tuberculosis*-infected mouse showing stomach and thyroid uptake only. Coronal and sagittal views of **c** healthy and **d** infected, respectively, mouse uptake at 48 h showing clearance of uptake from all tissues except thyroid.

SPECT images, are due to signal density (contrast) tissue differences and incomplete field of view. Finally, fluorescence microscopy of lung sections showing the distribution of 3d29 antibody in infected and healthy lungs showed intense 3d29 staining of all cuboidal CD68+ type II pneumocytes (Fig. 5a, arrows) and alveolar macrophages (arrowheads) in infected lungs. In healthy lungs (Fig. 5b), sparse staining with 3d29 was observed in type II

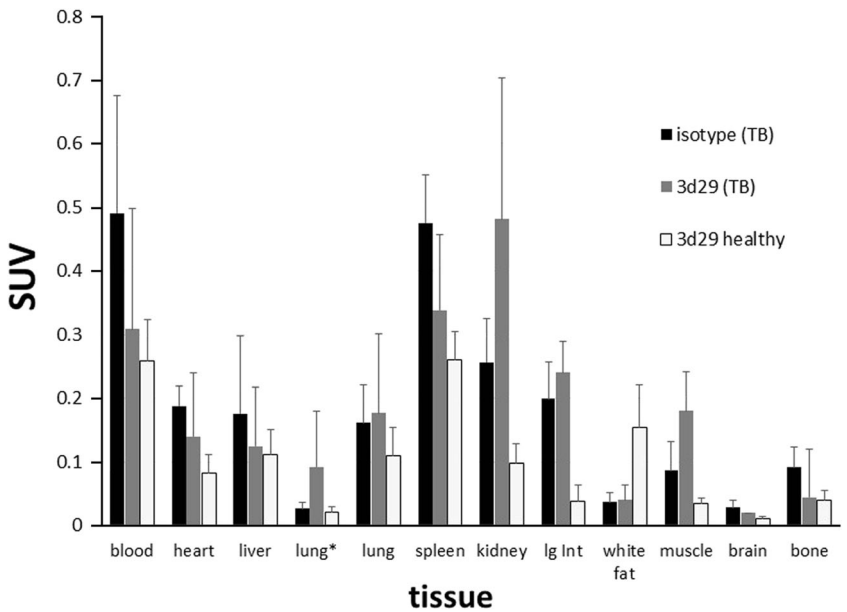


**Fig. 4.** *Ex vivo* biodistribution of [$^{125}$I]3d29 and [$^{125}$I]IgG$_{2a}$ isotype in *M. tuberculosis* infected and healthy mice at 24 h post-injection. Three mice from each group were injected with 15 μCi and sacrificed 24 h later by cervical dislocation. Selected organs were rapidly removed, weighed, disinfected, and counted the following day. Data are expressed as SUV except where indicated. Percent injected dose per organ was calculated for lungs to normalize for substantial edema.

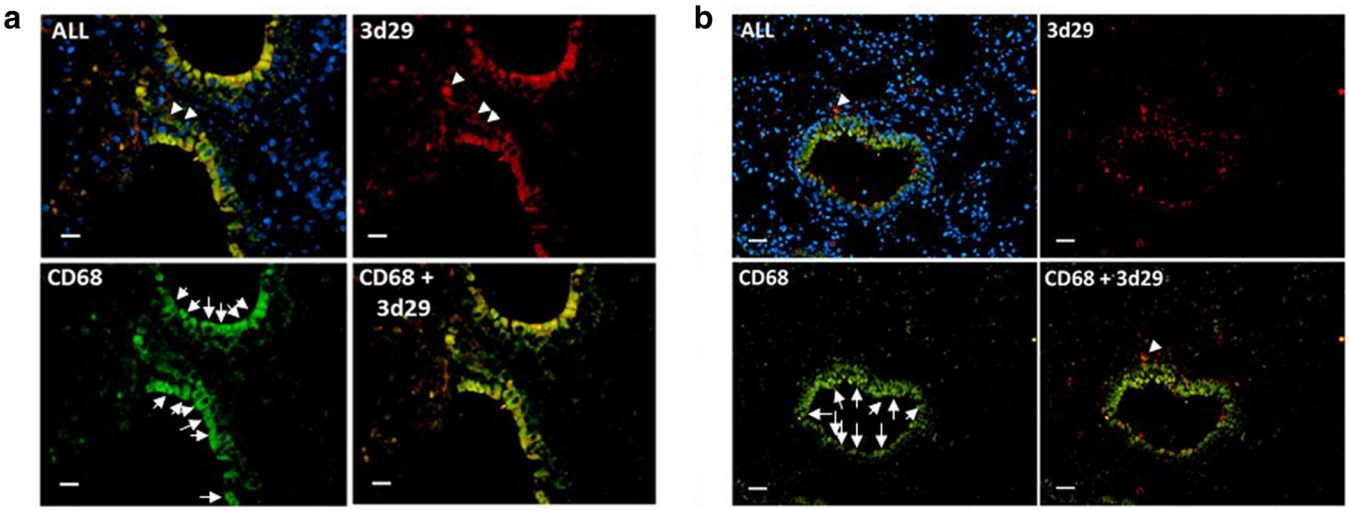


**Fig. 5.** Immunofluorescence microscopy in lung tissue from mice either **a** infected with *M. tuberculosis*. or **b** healthy mice. Infected lung sections were probed with 3d29, Hoechst 33342 nuclear stain and anti-CD68 to delineate all macrophages. Panels are as indicated. 3d29 staining (red) is densely associated with alveolar macrophages (CD68+, green, white arrows) in infected lungs while non-*M. tuberculosis*-infected alveoli are associated with sparse deposition of 3d29. Scale bar = 25 μm.

pneumocytes (arrows), with staining within a single alveolar macrophage also observed (arrowhead).

*M. tuberculosis* has eluded direct detection *in vivo* due to the presence of protective host factors such as granuloma formation and *Mycobacterium*-specific factors such as sequestration within phagocytes and cell wall biochemistry. That has challenged both small molecule ligand and specific antibody development. Efforts to harness *Mycobacteria*-specific siderophores as imaging agents have met with limited success due to the presence of highly lipophilic aliphatic tails, which impair aqueous solubility as well as favorable biodistribution [27–30]. That very property has, however, led to a sensitive *in vitro* assay for *M. tuberculosis* infection by detecting mycobactin-T from plasma or sputum [31]. *In vivo* detection of tuberculosis has focused on anatomic properties discerned by CT or magnetic resonance imaging [32–35] and host factors such as glycolytic metabolism using 2-deoxy-[$^{18}$F]fluoro-D-glucose ([$^{18}$F]FDG) positron emission tomography (PET), which detects both the metabolism of mycobacteria and the host immune response [36–40]. [$^{18}$F]FDG PET is the most widely used clinically approved method to molecularly image active TB [41], but suffers from potential misdiagnosis in the presence of malignancies such as carcinoma or lymphoma or in the presence of other infectious or granulomatous processes such as aspergillosis or sarcoid, and cannot accurately detect inactive or small lesions [37, 42, 43]. Other radiotracers that have been used clinically to image TB disease using SPECT include [$^{201}$Tl]$TlCl_3$, [$^{99m}$Tc]tetrafosmin, and [$^{99m}$Tc]sestamibi to compare perfusion and washout of radiotracer from suspected lesions and [$^{67}$Ga]Ga citrate, which accumulates in cells where iron is actively taken up such as bacteria, leukocytes, and tumors [44]. Each of those radiotracers, however, either necessitates early and delayed imaging to obtain a diagnosis by exclusion or is not specific for infection in the context of active malignancies as with gallium scintigraphy [43]. Recently, there has been increasing interest in developing bacteria-specific imaging agents for infections [45–49]. 2-[$^{18}$F]F-PABA has also been described as a bacteria-specific agent with the potential to image *M. tuberculosis* [50]. Other emerging translatable pre-clinical imaging methods for TB host response include Na[$^{18}$F]F PET/CT for imaging of calcifications within pulmonary granulomas [51], [$^{99m}$Tc]EDDA-tricine-HYNIC-Tyr3-octreotate SPECT to distinguish active from inactive TB lesions [52], [$^{64}$Cu]ATSM PET/CT to image hypoxia within granulomatous lesions [14], and [$^{123/4}$I]iodo-DPA-713 PET or SPECT/CT to image activated macrophages in any tissue compartment including CNS [53, 54]. While each of those techniques is an advancement forward towards delineation of aspects of TB, none is able to report on the most useful aspects of the disease, which include living bacterial burden and activation of adaptive immunological responses.

Complement 3d imaging represents an excellent opportunity to detect directly live *M. tuberculosis*, as ubiquitous C3 is cleaved by *M. tuberculosis* down to covalently bound C3d on its cell surface [6]. The complement cascade is diverse but selective in the resulting complement species according to the molecular environment. Since *M. tuberculosis* organisms are readily phagocytosed by pneumocytes and alveolar and parenchymal macrophages [55, 56], the window of opportunity for imaging with radiolabeled antibodies captures living mycobacteria that persist in the extracellular space (therapeutically accessible mycobacteria) as well as those newly ingested by phagocytes (persistent mycobacteria). Dormant TB, in which mycobacteria are presumably inactive and sequestered

within host cells, may not be available for detection with radiolabeled 3d29, but reactivation of disease will result in release of active *M. tuberculosis* from burst host cells, allowing detection of recrudescence using this method. Because the technique requires 24 h to acquire data, and data include uptake over the entire body, it may be more useful than sputum tests in regions where SPECT devices are present, which includes centers in India, China, and South Africa, where prevalence of TB is high. More so than diagnosis, the decision to continue treatment could be augmented by imaging where both the treating physician and patient can rapidly see a picture delineating the extent of remaining infection. Local governments and communities have a vested interest in patient compliance with treatment regimens. Comparatively, rapid *M. tuberculosis*-targeted imaging of the entire body may help increase compliance in the developing world.

## Conclusions

Our results demonstrate that radiolabeled 3d29 can be used to detect and localize areas of infection with *M. tuberculosis* non-invasively by 24 h after radiotracer injection. By comparison, radiolabeled isotype control could not discern normal from infected tissues.

*Acknowledgements.* We would like to acknowledge Mariah Klunk for operating the scanner.

**Funding Information** The authors would like to acknowledge funding from the following sources: JHU Musculoskeletal Research Award (CAF), R01 EB020539 (SKJ), P41 EB024495 (MGP), The Stabler Foundation (MGP), and the Alliance for Lupus Research (VMH).

#### Compliance with Ethical Standards

#### *Conflict of Interest*

The authors declare that they have no conflict of interest.

## References

1. WHO Global tuberculosis report 2016. http://www.who.int/tb/publications/global_report/gtbr2016_executive_summary.pdf?ua=1 (accessed December 29, 2016).
2. VanderVen BC, Huang L, Rohde KH, Russell DG (2016) The minimal unit of infection: mycobacterium tuberculosis in the macrophage. Microbiol Spectr 4. doi: 10.1128/microbiolspec.TBTB2-0025-2016
3. Mace LS (1908) Review of recent work on tuberculosis. Cal State J Med 6:298–301
4. Freund A (1946) Tuberculosis and non-tuberculous lung diseases: a critical review of the literature of the last years. Acta Med Orient 5:305–315
5. Mathe CP (1946) Unilateral renal tuberculosis; management of the nephrectomized patient: review of ninety-eight cases. Trans West Sect Am Urol Assoc 13:31–38
6. Merle NS, Noe R, Halbwachs-Mecarelli L, Fremeaux-Bacchi V, Roumenina LT (2015) Complement system part II: role in immunity. Front Immunol 6: doi: 10.3389/fimmu.2015.00257
7. Bergmann-Leitner ES, Leitner WW, Tsokos GC (2006) Complement 3d: from molecular adjuvant to target of immune escape mechanisms. Clin Immunol 121:177–185
8. Gou SJ, Yuan J, Wang C, Zhao MH, Chen M (2013) Alternative complement pathway activation products in urine and kidneys of patients with ANCA-associated GN. Clin J Am Soc Nephrol 8:1884–1891
9. Thurman JM, Kulik L, Orth H, Wong M, Renner B, Sargsyan SA, Mitchell LM, Hourcade DE, Hannan JP, Kovacs JM, Coughlin B, Woodell AS, Pickering MC, Rohrer B, Holers VM (2013) Detection of complement activation using monoclonal antibodies against C3d. J Clin Invest 123:2218–2230
10. Borschukova O, Paz Z, Ghiran IC, Liu CC, Kao AH, Manzi S, Ahearn JM, Tsokos GC (2012) Complement fragment C3d is colocalized within the lipid rafts of T cells and promotes cytokine production. Lupus 21:1294–1304
11. Sargsyan SA, Serkova NJ, Renner B, Hasebroock KM, Larsen B, Stoldt C, McFann K, Pickering MC, Thurman JM (2012) Detection of glomerular complement C3 fragments by magnetic resonance imaging in murine lupus nephritis. Kidney Int 81:152–159
12. Wouters D, Wiessenberg HD, Hart M, Bruins P, Voskuyl A, Daha MR, Hack CE (2005) Complexes between C1q and C3 or C4: novel and specific markers for classical complement pathway activation. J Immunol Methods 298:35–45
13. Ristau T, Paun C, Ersoy L, Hahn M, Lechanteur Y, Hoyng C, de Jong EK, Daha MR, Kirchhof B, den Hollander AI, Fauser S (2014) Impact of the common genetic associations of age-related macular degeneration upon systemic complement component C3d levels. PLoS One 9:e93459
14. Harper J, Skerry C, Davis SL, Tasneen R, Weir M, Kramnik I, Bishai WR, Pomper MG, Nuermberger EL, Jain SK (2012) Mouse model of necrotic tuberculosis granulomas develops hypoxic lesions. J Infect Dis 205:595–602
15. Ordonez AA, Tasneen R, Pokkali S, Xu Z, Converse PJ, Klunk MH, Mollura DJ, Nuermberger EL, Jain SK (2016) Mouse model of pulmonary cavitary tuberculosis and expression of matrix metalloproteinase-9. Dis Models Mech 9:779–788
16. Haisma HJ, Hilgers J, Zurawski VR Jr (1986) Iodination of monoclonal antibodies for diagnosis and radiotherapy using a convenient one vial method. J Nucl Med 27:1890–1895
17. Weinstein EA, Liu L, Ordonez AA, Wang H, Hooker JM, Tonge PJ, Jain SK (2012) Noninvasive determination of 2-[$^{18}$F]-fluoroisonicotinic acid hydrazide pharmacokinetics by positron emission tomography in Mycobacterium tuberculosis-infected mice. Antimicrob Agents Chemother 56:6284–6290
18. Vaidyanathan G, Zalutsky MR (1990) Radioiodination of antibodies via N-succinimidyl 2,4-dimethoxy-3-(trialkylstannyl)benzoates. Bioconjug Chem 1:387–393
19. Hnatowich DJ (1990) Recent developments in the radiolabeling of antibodies with iodine, indium, and technetium. Semin Nucl Med 20:80–91
20. Turner CJ, Sykes TR, Longenecker BM, Noujaim AA (1988) Comparative radiolabeling and distribution of a tumour-directed monoclonal antibody. Int J Rad Appl Instrum B 15:701–706
21. Garg PK, Alston KL, Welsh PC, Zalutsky MR (1996) Enhanced binding and inertness to dehalogenation of alpha-melanotropic peptides labeled using N-succinimidyl 3-iodobenzoate. Bioconjug Chem 7:233–239
22. Leiter EH (1988) Control of spontaneous glucose intolerance, hyperinsulinemia, and islet hyperplasia in nonobese C3H.SW male mice by Y-linked locus and adrenal gland. Metabolism 37:689–696
23. Stanton LA, Fenhalls G, Lucas A, Gough P, Greaves DR, Mahoney JA, Helden Pv, Gordon S (2003) Immunophenotyping of macrophages in human pulmonary tuberculosis and sarcoidosis. Int J Exp Pathol 84:289–304
24. Scordo JM, Knoell DL, Torrelles JB (2016) Alveolar epithelial cells in Mycobacterium tuberculosis infection: active players or innocent bystanders? J Innate Immun 8:3–14
25. Fehrenbach H (2001) Alveolar epithelial type II cell: defender of the alveolus revisited. Respir Res 2:33–46
26. Renner B, Strassheim D, Amura CR, Kulik L, Ljubanovic D, Glogowska MJ, Takahashi K, Carroll MC, Holers VM, Thurman JM (2010) B cell subsets contribute to renal injury and renal protection after ischemia/reperfusion. J Immunol 185:4393–4400
27. Petrik M, Zhai C, Novy Z, Urbanek L, Haas H, Decristoforo C (2016) In vitro and in vivo comparison of selected Ga-68 and Zr-89 labelled siderophores. Mol Imaging Biol 18:344–352
28. Zhai C, Summer D, Rangger C, Haas H, Haubner R, Decristoforo C (2015) Fusarinine C, a novel siderophore-based bifunctional chelator for radiolabeling with gallium-68. J Label Compd Radiopharm 58:209–214

29. Petrik M, Franssen GM, Haas H, Laverman P, Hörtnagl C, Schrettl M, Helbok A, Lass-Flörl C, Decristoforo C (2012) Preclinical evaluation of two 68Ga-siderophores as potential radiopharmaceuticals for Aspergillus fumigatus infection imaging. Eur J Nucl Med Mol Imaging 39:1175–1183
30. Petrik M, Haas H, Dobrozemsky G, Lass-Florl C, Helbok A, Blatzer M, Dietrich H, Decristoforo C (2010) 68Ga-siderophores for PET imaging of invasive pulmonary aspergillosis: proof of principle. J Nucl Med 51:639–645
31. Sakamuri RM, Capek P, Dickerson TJ, Barry CE III, Mukundan H, Swanson BI (2014) Detection of stealthy small amphiphilic biomarkers. J Microbiol Methods 103:112–117
32. Park S, Hong YK, Joo SH, Choe KO, Cho SH (1999) CT findings of pulmonary tuberculosis presenting as segmental consolidation. J Comput Assist Tomogr 23:736–742
33. Brizi MG, Celi G, Scaldazza AV, Barbaro B (1998) Diagnostic imaging of abdominal tuberculosis: gastrointestinal tract, peritoneum. Lymph Nodes Rays 23:115–125
34. Sharif HS, Morgan JL, al Shahed MS, al Thagafi MY (1995) Role of CT and MR imaging in the management of tuberculous spondylitis. Radiol Clin N Am 33:787–804
35. Kuhlman JE, Deutsch JH, Fishman EK, Siegelman SS (1990) CT features of thoracic mycobacterial disease. Radiographics 10:413–431
36. Ankrah AO, van der Werf TS, de Vries EF et al (2016) PET/CT imaging of Mycobacterium tuberculosis infection. Clin Transl Imaging 4:131–144
37. Balogova S, Talbot JN, Nataf V, Michaud L, Huchet V, Kerrou K, Montravers F (2013) 18F-fluorodihydroxyphenylalanine vs other radiopharmaceuticals for imaging neuroendocrine tumours according to their type. Eur J Nucl Med Mol Imaging 40:943–966
38. Kosterink JG (2011) Positron emission tomography in the diagnosis and treatment management of tuberculosis. Curr Pharm Des 17:2875–2880
39. Davis SL, Nuermberger EL, Um PK, Vidal C, Jedynak B, Pomper MG, Bishai WR, Jain SK (2009) Noninvasive pulmonary [$^{18}$F]-2-fluoro-deoxy-D-glucose positron emission tomography correlates with bactericidal activity of tuberculosis drug treatment. Antimicrob Agents Chemother 53:4879–4884
40. Murawski AM, Gurbani S, Harper JS, Klunk M, Younes L, Jain SK, Jedynak BM (2014) Imaging the evolution of reactivation pulmonary tuberculosis in mice using $^{18}$F-FDG PET. J Nucl Med 55:1726–1729
41. Gambhir S, Ravina M, Rangan K, Dixit M, Barai S, Bomanji J, International Atomic Energy Agency Extra-pulmonary TB Consortium (2017) Imaging in extrapulmonary tuberculosis. Int J Infect Dis 56:237–247
42. Sathekge M, Maes A, D'Asseler Y, Vorster M, Van de Wiele C (2012) Nuclear medicine imaging in tuberculosis using commercially available radiopharmaceuticals. Nucl Med Commun 33:581–590
43. Vorster M, Sathekge MM, Bomanji J (2014) Advances in imaging of tuberculosis: the role of $^{18}$F-FDG PET and PET/CT. Curr Opin Pulm Med 20:287–293
44. Cooke SG, Davies ER, Goddard PR (1989) Pulmonary uptake in 67-gallium citrate scintigraphy-the 'negative heart' sign. Postgrad Med J 65:885–891
45. Davis SL, Be NA, Lamichhane G, Nimmagadda S, Pomper MG, Bishai WR, Jain SK (2009) Bacterial thymidine kinase as a non-invasive imaging reporter for Mycobacterium tuberculosis in live animals. PLoS One 4:e6297
46. Gowrishankar G, Namavari M, Jouannot EB, Hoehne A, Reeves R, Hardy J, Gambhir SS (2014) Investigation of 6-[$^{18}$F]-fluoromaltose as a novel PET tracer for imaging bacterial infection. PLoS One 9:e107951
47. Boegemann M, Schrader AJ, Krabbe LM, Herrmann E (2015) Present, emerging and possible future biomarkers in castration resistant prostate cancer (CRPC). Curr Cancer Drug Targets 15:243–255
48. Weinstein EA, Ordonez AA, DeMarco VP et al (2014) Imaging Enterobacteriaceae infection in vivo with 18F-fluorodeoxysorbitol positron emission tomography. Sci Transl Med 6:259ra146
49. Jain SK (2017) The promise of molecular imaging in the study and treatment of infectious diseases. Mol Imaging Biol 19:341–347
50. Ordonez AA, Weinstein EA, Bambarger LE, Saini V, Chang YS, DeMarco VP, Klunk MH, Urbanowski ME, Moulton KL, Murawski AM, Pokkali S, Kalinda AS, Jain SK (2017) A systematic approach for developing bacteria-specific imaging tracers. J Nucl Med 58:144–150
51. Ordonez AA, DeMarco VP, Klunk MH et al (2015) Imaging chronic tuberculous lesions using sodium [$^{18}$F]fluoride positron emission tomography in mice. Mol Imaging Biol 17:609–614
52. Ahmadihosseini H, Abedi J, Ghodsi Rad MA, Zakavi SR, Knoll P, Mirzaei S, Sadeghi R (2014) Diagnostic utility of 99mTc-EDDA-tricine-HYNIC-Tyr3-octreotate SPECT for differentiation of active from inactive pulmonary tuberculosis. Nucl Med Commun 35:1262–1267
53. Foss CA, Harper JS, Wang H, Pomper MG, Jain SK (2013) Noninvasive molecular imaging of tuberculosis-associated inflammation with radioiodinated DPA-713. J Infect Dis 208:2067–2074
54. Ordonez AA, Pokkali S, DeMarco VP et al (2015) Radioiodinated DPA-713 imaging correlates with bactericidal activity of tuberculosis treatments in mice. Antimicrob Agents Chemother 59:642–649
55. Songane M, Kleinnijenhuis J, Netea MG, van Crevel R (2012) The role of autophagy in host defence against Mycobacterium tuberculosis infection. Tuberculosis (Edinb) 92:388–396
56. Deretic V, Singh S, Master S, Harris J, Roberts E, Kyei G, Davis A, de Haro S, Naylor J, Lee HH, Vergne I (2006) Mycobacterium tuberculosis inhibition of phagolysosome biogenesis and autophagy as a host defence mechanism. Cell Microbiol 8:719–727